Mechanics & Industry **26**, 15 (2025)

https://doi.org/10.1051/meca/2025010

Mechanics & Industry

Available online at:
www.mechanics-industry.org

ORIGINAL ARTICLE

Influence of Electric Cylinder Transmission Characteristics on Servo System

Yang Lei[1,2,*], Yuanqing Xia[1], and Yiyang Huo[2]

[1] School of Automation, Beijing Institute of Technology, Beijing 100081, PR China
[2] China North Vehicle Research Institute, Beijing 100072, China

Received: 3 December 2024 / Accepted: 10 March 2025

Abstract. Aiming at the problem that the servo control accuracy is restricted by the mechanical transmission characteristics of the electric cylinder, the servo motor model, the drive model and the servo control system model of the electric cylinder are established in this paper. The test bench system of mechanical parameters of electric cylinder was built. The key mechanical transmission parameters of the electric cylinder are obtained through the accurate parameter measurement of the actual system. Based on the measured data, the model is modified, and then the nonlinear model of electric cylinder servo system is constructed, which the empty return clearance and stiffness are considered in the model. This model is used to deeply analyse the influence of the mechanical transmission of electric cylinder on the servo system error, and reveal the sensitivity relationship between the clearance and stiffness on the servo system accuracy. The conclusion provides a scientific basis for the optimisation design of servo system based on electric cylinder. It has important theoretical and practical significance for improving servo control accuracy.

Keywords: Electric cylinders / empty return clearance / stiffness / servo system

1 Introduction

Electric cylinder is a modular product that integrates servo motor and lead screw, and is also an executive element that provides linear motion and thrust [1,2]. The schematic diagram of the servo system based on the electric cylinder is shown in Fig. 1. Its working principle is to convert the rotating motion of the servo motor through the lead screw into the linear reciprocating motion of the push rod, and drive the load through the push rod. The precise position control is realised by using the control characteristics of servo motor [3,4]. Compared with the traditional hydraulic cylinder servo system, the servo system based on the electric cylinder has the advantages of high precision, fast response speed, not be affected by environmental changes such as temperature, and easy to maintain [5]. The electric cylinder servo system is widely used in aerospace simulator, weapon launch stability platform, printing press and medical equipment [6,9].

With the further improvement of the position accuracy and dynamic response process of the servo system based on electric cylinder, the electric cylinder cannot only be regarded as a linear system with simplified transmission, but its nonlinear mechanical characteristics—such as empty return clearance, stiffness and hysteresis are gradually exposed. The mechanical transmission characteristics of the electric cylinder will restrict the design of the servo control system and affect the improvement of the servo accuracy of the system [10,14]. Reference [10] highlights that the nonlinear factors inside the transmission mechanism have an important impact on the system performance. Although it mainly focuses on hydraulic cylinder models, it has begun to notice the existence of nonlinear factors such as empty return clearance and tries to take them into account in the modelling process. This suggests that we should analyse these nonlinear factors more comprehensively in the follow-up research. Reference [11], the nonlinear part of the electric cylinder is equivalent to a nonlinear disturbance as a whole, and a LuGre friction model is synthesised by all the perturbations. However, this method ignores the influence of the gap, which restricts the improvement of servo accuracy in the design of high-precision servo system. Reference [12], the effect of strong nonlinearity of the gap was analysed, and a fuzzy adaptive PID control was designed to compensate for this effect. Reference [13], the motion characteristics of the actuator under different stiffness states were analysed, and expectations were put forward for its high-precision performance in cooperation with the control system. In summary, a large number of scholars have studied the effect of electric cylinder on servo system mainly on

* e-mail: tylqa@163.com

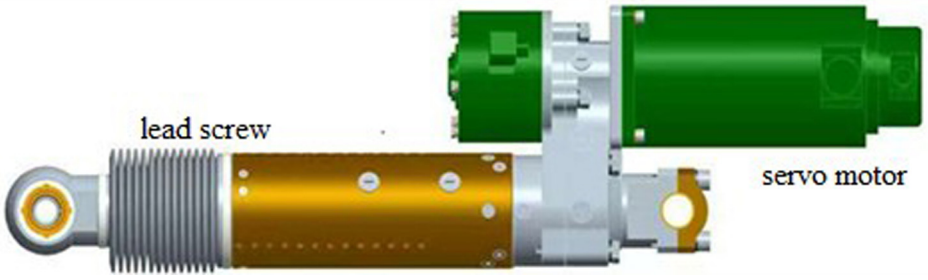

Fig 1. Schematic diagram of the electric cylinder and its servo components.

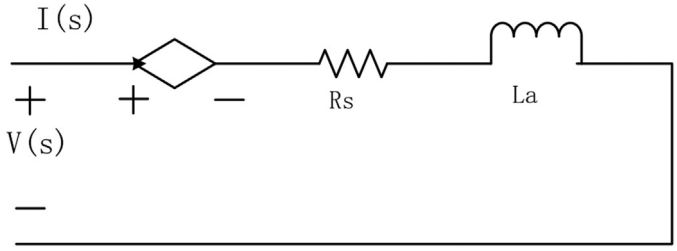

Fig. 2. Equivalent circuit diagram of permanent magnet synchronous motor model.

nonlinear clearance and stiffness. However, there is no in-depth study on the physical model of clearance and stiffness and how to test and calibrate the actual system, how to modify the simulation model, and the sensitivity analysis of clearance and stiffness to the accuracy of the servo system. To improve the reliability and practicability of the model, it is necessary to modify the model parameters more comprehensively through the experimental data.

A servo motor model, a drive model and a servo control system model of the electric cylinder are first established, and then the key parameters of the electric cylinder are determined through experiments. Based on the experimental results, a nonlinear model of the electric cylinder servo system considering the empty return clearance and stiffness is established. The error source of servo system with electric cylinder mechanical transmission is analysed using this model. Finally, the sensitivity relationship between the empty return clearance and stiffness of electric cylinder to system error is obtained. The results can guide the optimisation design of servo systems based on electric cylinders.

2 Model Building

2.1 Mathematical model of electric cylinder motor

Servo motor is often used for accurate position control in servo system [15,16]. Most servomotors are permanent magnet synchronous motors [17,19]. We present a mathematical model of a permanent magnet synchronous motor based on electric cylinder. This model can be realised by establishing its voltage, flux torque and motion equations. The voltage equation is as follows:

$$\begin{bmatrix} u_q \\ u_d \end{bmatrix} = \begin{bmatrix} R_s + L_a p & \omega_r L_a \\ -\omega_r L_a & R_s + L_a p \end{bmatrix} \begin{bmatrix} i_q \\ i_d \end{bmatrix} + \begin{bmatrix} \omega_r \phi_f \\ 0 \end{bmatrix}. \quad (1)$$

The instantaneous torque is calculated as follows:

$$T_{em} = {}^{em} K_t i_q = T_l + B\Omega_r + Jp\Omega_r, \quad (2)$$

where R_s is the stator resistance, L_a is the armature inductance (The salient pole effect is not considered, and d-axis and q-axis inductances of the permanent magnet synchronous motor are simplified to be equal.); J is the moment of inertia of the motor; ϕ_f is the magnetic flux generated by permanent magnets (ϕ_f is constant); ω_r is the angular frequency of the rotor; B is the viscous friction coefficient; p is the differential operator; T_l is the load torque; K_t is the torque coefficient; u_d,u_q,i_d and i_q are the voltage and current of the axes and q-axes, and $\boldsymbol{\Omega}_r$ is the angular velocity of the rotor.

The servo system adopts $i_d = 0$ control mode for permanent magnet synchronous motor control.

Substituting $i_d = 0$ into Eq. (1), we have:

$$\begin{aligned} u_d &= -\omega_r L_a i_q \\ u_q &= R_s i_q + L_a p i_q + \omega_r \phi_f \end{aligned}. \quad (3)$$

According to the permanent magnet synchronous motor model in Equation (3), a first-order series circuit can be equivalently derived, as shown in Fig. 2. The circuit is composed of a resistor, an inductor and a back potential voltage source. It is assumed that the back potential voltage is now constant, since the back potential voltage

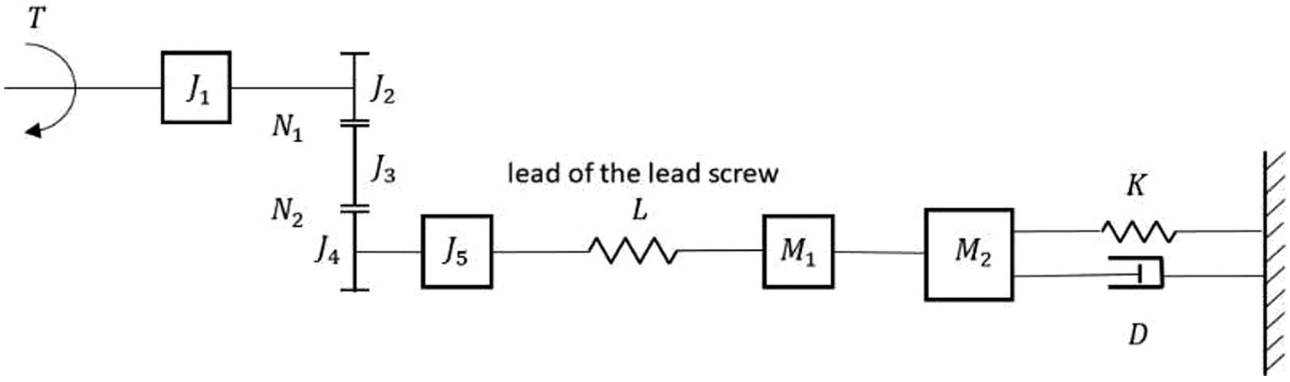

Fig. 3. Schematic diagram of the electric cylinder internal structure and load.

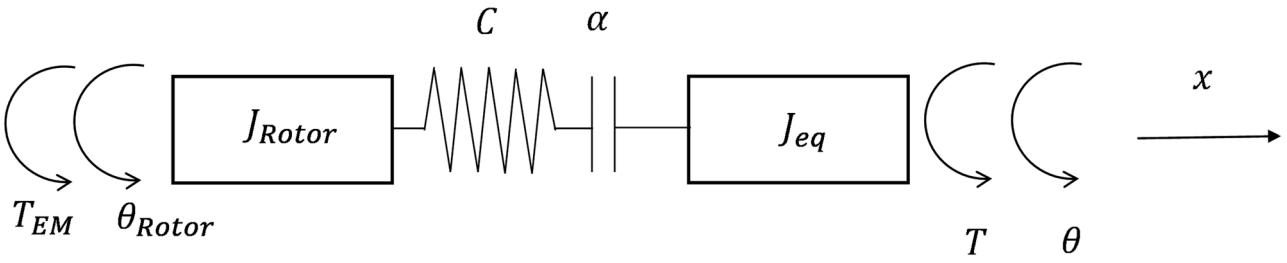

Fig. 4. Double inertia model considering clearance and stiffness.

usually changes slowly relative to the current. The small signal transfer function from the Q-axis voltage to the Q-axis current of the motor can be obtained by using the method of small signal circuit analysis and Laplace change of the circuit.

$$\frac{I_q(s)}{U_q(s)} = \frac{\frac{1}{R_s}}{\left(1+\frac{L_a}{R_s}s\right)} = \frac{1}{L_a s + R_s}. \tag{4}$$

2.2 Transmission model of the electric cylinder

The drive part of the electric cylinder is mainly composed of a two-stage reduction gear and a planetary roller lead screw, forming in series [20]. The load of the servo system is converted to the output end of the electric cylinder, and its internal structure is shown in Fig. 3.

where, T is the output torque of the servo motor; J_1, J_2, J_3, J_4 and J_5 are respectively the moment of inertia of the motor rotor, gear 1, gear 2, and gear 3, and the rotating part of the planetary roller screw; M_1 is the mass of the planetary roller lead screw nut and push rod. M_2 is the equivalent mass of the load converted to the output of the electric cylinder; K and D are the equivalent stiffness and damping of the load converted to the output end of the electric cylinder, respectively; L is the lead of the lead screw; N_1 and N_2 are the reduction ratios of the two gear pairs, respectively.

When the clearance and stiffness are considered based on Fig. 3, the electric cylinder can be equivalent to a double inertia system. Its principle is shown in Fig. 4.

where, J_{Rotor} represents the moment of inertia of the motor rotor; J_{eq} represents the equivalent moment of inertia of the screw nut, push rod, lead rod, reduction gear and shafting equivalent to the motor rotor shaft; θ_{Rotor}, T_{EM} are the rotor angles of the motor and output torque of the motor, respectively; θ and T are the rotation angles of the equivalent inertia and the torque load, respectively; x is the axial displacement after reducing deceleration ratio and lead; C is the forward composite stiffness, and α is the estimated forward pass gap. The dead-time model is used to describe the torque relationship between the two inertias:

$$T = \begin{cases} C\left(\Delta\theta - \frac{\alpha}{2}\right), \Delta\theta > \frac{\alpha}{2} \\ 0, -\frac{\alpha}{2} < \Delta\theta < \frac{\alpha}{2} \\ C\left(\Delta\theta + \frac{\alpha}{2}\right), \Delta\theta < -\frac{\alpha}{2} \end{cases}. \tag{5}$$

$$T = J_{eq}\theta$$

where, $\Delta\theta = \theta_{Rotor} - \theta$

2.3 Model of servo control system

The servo system based on the electric cylinder is used for precise position control, employing the three closed-loop control modes: position ring, speed ring and current ring. The control principal diagram is shown in Fig. 5.

Position ring, speed ring and current ring are controlled by PI controller. The S-domain transfer function of the PI controller is as follows:

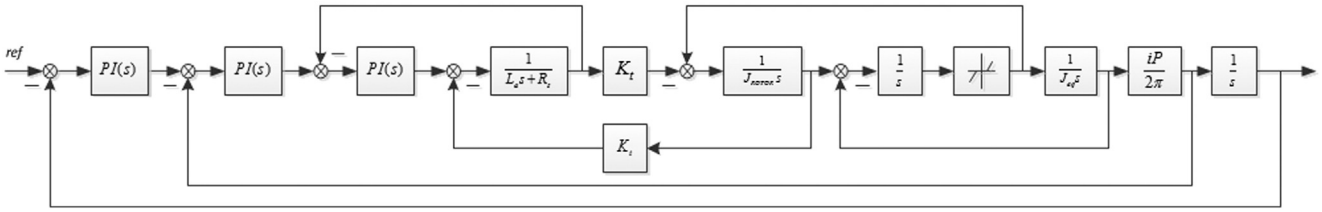

Fig. 6. Mathematical model of the electric cylinder servo system based on Simulink.

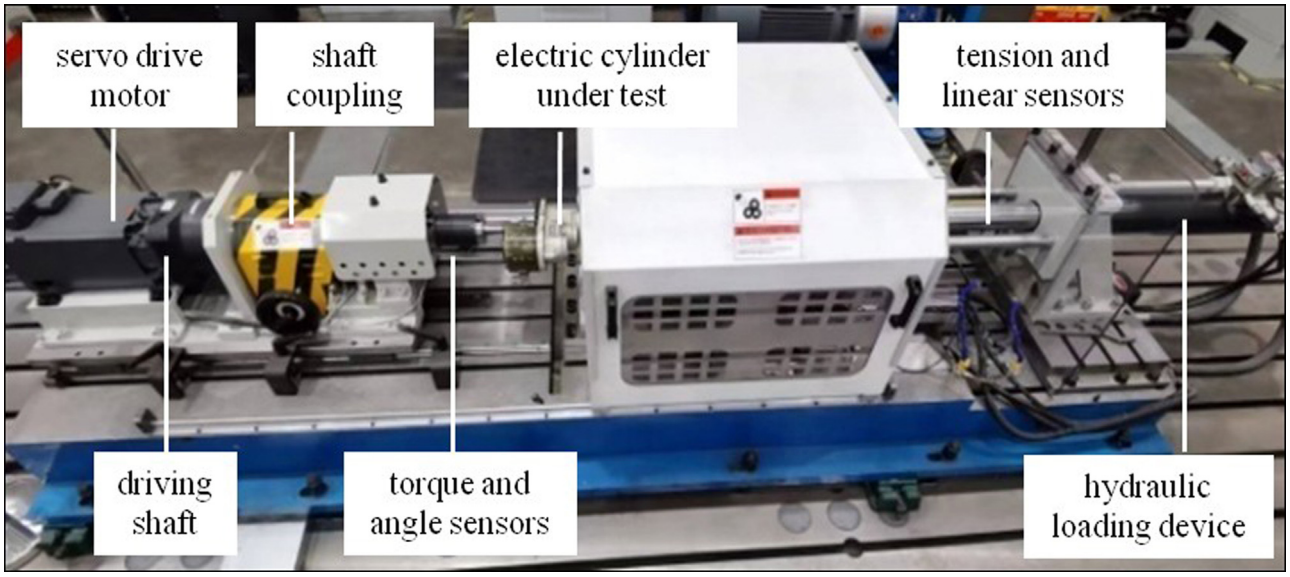

Fig. 7. Composition of the electric cylinder mechanical characteristics test bench.

$$PI(\mathrm{s}) = \frac{K_\mathrm{p} * K_\mathrm{i}}{\mathrm{s}} + K_\mathrm{p} = \frac{K_\mathrm{p} * K_\mathrm{i}(1+\frac{s}{K_\mathrm{i}})}{s}. \quad (6)$$

Based on the motor and mechanical transmission models of the electric cylinder established in sections 2.1 and 2.2, combined with Eq. (6), the overall servo control system model based on the electric cylinder is constructed. The block diagram of the model based on Matlab/Simulink is shown in Fig. 6.

3 Calculation of model parameters

Based on the double inertia model, two important parameters: clearance and stiffness need to be obtained for the electric cylinder transmission model.

3.1 Test bench for obtaining key parameters of the electric cylinder

The approach to determining the clearance and stiffness of the electric cylinder is: for the forward and reverse loading and unloading of the electric cylinder, the displacement of the electric cylinder transmission system relative to the load force or moment will form a closed curve, that is, a hysteresis curve. Then, based on the hysteresis curve, the empty return clearance and elastic deformation stiffness of the electric cylinder can be obtained. On this basis, an electric cylinder test bench is established. The complete test bench for the mechanical characteristics of the electric cylinder is shown in Fig. 7.

The test bench mainly composed of servo drive motor, transmission shaft, coupling, the electric cylinder to be tested, hydraulic loading device, and sensors. The basic principle of the test is: first, the locking gear is installed to lock the output end. Then, the servo motor is gradually loaded to the rated torque from no-load through computer control of the frequency converter. The input torque on the shaft will be measured by the torque sensor. The torsion angle of the shaft will be measured by the angle sensor. Finally, the data collected by the sensors will be transmitted to the host computer for processing and analysis. On the test bench, a torquemeter is for accurate measurement. The high-precision grating angle sensor is used to measure the torsion angle of the drive shaft. The tension pressure sensor is used to measure the axial force on the output side of the electric cylinder. The linear grating is used to measure the displacement on the output side. The resolutions of the torquemeter, high-precision grating angle sensor, tension pressure sensor, and linear grating are ± 0.4 Nm, ± 2 ", ± 1 N, and ± 0.005 mm.

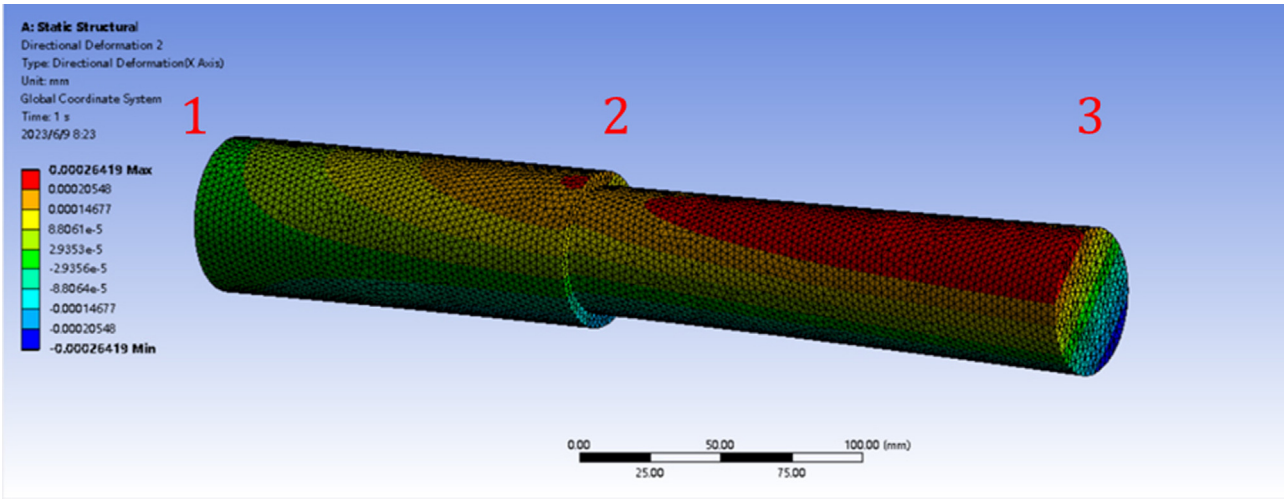

Fig. 8. Strain cloud diagram of the input shaft under torque load.

3.2 Error analysis of the test bench for the electric cylinder mechanical characteristics

In addition to installing the above torquemeter and grating angle sensor between the input side and the drive motor of the electric cylinder mechanical characteristics test bench, additional elastic couplings should be installed to compensate for the concentricity error caused by machining and assembly of the test bench. It results in a longer input shaft between the angle grating and the input gear. The strain generated by the torque of the input shaft may be superimposed with the angle inside the electric cylinder, which will affect the accuracy of angle measurement. Therefore, it is necessary to analyse the torsion error of the input shaft to ensure that the angle measured by the grating is consistent with the actual angle of the electric cylinder.

Since part of the input shaft is covered by a protective cover, it is impossible to measure the deformation of the input shaft during the test by installing a strain gauge. Therefore, Ansys Workbench is used for finite element analysis on the input shaft to determine the maximum torsional deformation that may occur during the test and analyse the influence of deformation on angle measurement.

As shown in Fig. 8, section 1 is the position where the torque loading shaft of the test bench meshes with the electric cylinder input shaft through the gear. To simplify the calculation, the gear geometric features are removed, and fixed joint constraint is set on section 1 to simulate the fixed linear output end of the electric cylinder. The load torque of the motor shaft is the measured torque curve of the actual hysteresis test and ranges from 0 to 50 Nm. In addition to fixed joints and torque loads, the bearing reaction is also taken into account. Taking section 2 as an example, spring is used to connect the shaft and bearing chamber to approximate the reaction forces of an angular contact bearing. The radial stiffness is $3.789 \times 10^7 N/m$ and the axial stiffness is$1.165 \times 10^7 N/m$. Fig. 8 shows the normal deformation of the shaft after the loading torque reaches the maximum of 50 Nm. Section 3 is the installation position of the input shaft angle sensor. The maximum relative torsion deformation of the input shaft to section 1 is 1.362". The relative torsion angle between the angle sensor and section 1 is 0.94 "Both deformations are less than the resolution of the angle sensor. It can be considered that the torsion deformation of the input shaft has no effect on the measurement of the internal deformation of the electric cylinder.

In addition, in the test, the output side of the electric cylinder will bear a large push tension. The output side mounting seat may also be deformed under the influence of this thrust, which will reduce the measurement accuracy of the linear grating. In the test, a dial gauge is used to measure the axial deformation of the mounting base under the maximum load. During the test, the dial gauge reading is constant. It can be concluded that the deformation of the mounting seat in the test bench can be ignored, and the measured value of the linear grating is the displacement of the output side of the electric cylinder.

3.3 Calculation of empty return clearance and stiffness parameters of the electric cylinder

Due to the coupling of energy dissipation links such as air return clearance, elastic-plastic deformation, and friction, hysteresis characteristics are common in precision drives. It often shows that the unloading curve is not consistent with the loading curve, and the enclosed graph area formed by the two curves reflects the energy loss during loading and unloading process. The hysteresis curve of the motor cylinder with a torque load of $\pm$50Nm is shown in Fig. 9. It can be seen that the torsion angle has a sharp rise/fall process near the zero-torque point. This phenomenon reflects the empty travel inside the electric cylinder during load reversal, that is, the size of the backlash. At the end of the empty stroke, the driving part and the driven part begin to contact and transfer deformation torque. Due to

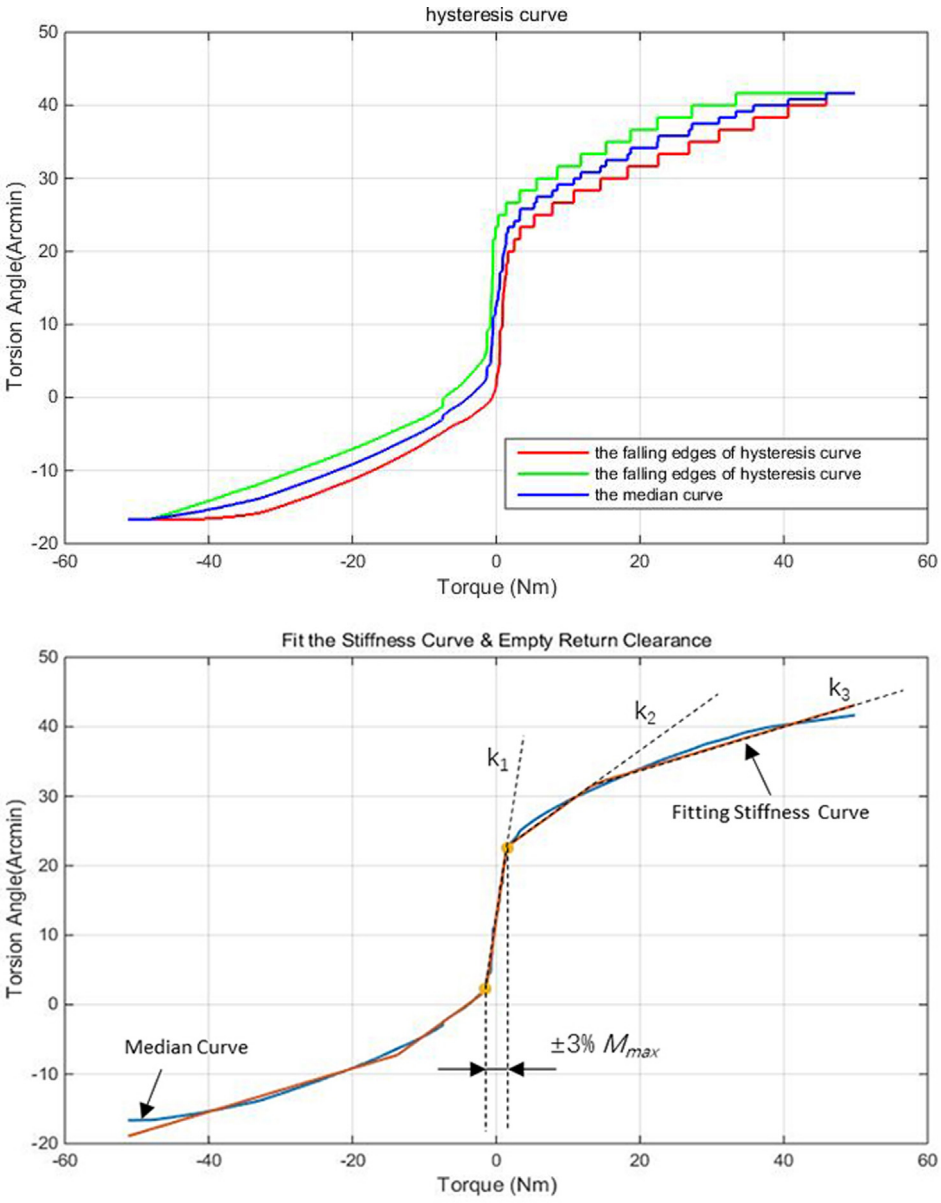

Fig. 9. Calculation diagram of hysteresis curve, empty return clearance and stiffness of electric cylinder.

the influence of the stiffness of transmission components, as the load increases, the torque angle of the electric cylinder increases more slowly than that in the no-travel stage.

Since it is impossible to directly calculate the void clearance and stiffness from the hysteresis loop, the median curve of hysteresis curve is used as the object. The median curve is obtained by averaging the rising and falling edges of hysteresis curve. In the experiment, gradient loading and unloading methods are used, and partial hysteresis curve are measured to obtain the median curve. The data smoothing method uses median filtering, that is, for a section of sampled data with the same torsion angle, only the data points corresponding to the median torque value are retained. The smoothed median curve is shown in Fig. 9.

Table 1. Fitting parameters

Parameters	Values
k_1	14.725 arcmin/N · m
k_2	0.529 arcmin/N · m
k_3	0.348 arcmin/N · m
T_1	1.491 N · m
T_2	17.23 N · m

The median curve is fitted by the superimposed polyline of three straight lines, which serves as the basis for subsequent calculation of backlash clearance and stiffness. The first section is used to estimate the backlash clearance,

Table 2. Simulation parameters of models

	Parameters	Parameter values
Motor controller	Position loop K_p	50 rad/m · s
	Position loop K_I	35 rad/m · s^2
	Speed loop K_p	100 A · s/rad
	Speed loop K_I	60 A/rad
	Current loop K_p	80 V/A
	Current loop K_I	50 V/A · s
Electromotor	Armature inductance L	2.26 mH
	Armature resistance R	0.73 Ω
	Torque coefficient K_t	0.716 N · m/A
	Counter electromotive force coefficient K_e	0.167 V · s/rad
	Rotational inertia of the rotor J_{Rotor}	4.45×10^{-4}kg · m^2
Driving mechanism	Gear ratio i	1/2.16
	Lead of the lead screw P	20 mm
	Combined stiffness C	See formula (5)
	Empty Return clearance α	20.15 arcmin
	Equivalent moment of inertia J_{eq}	1.783 × 10−3 kg.m 2

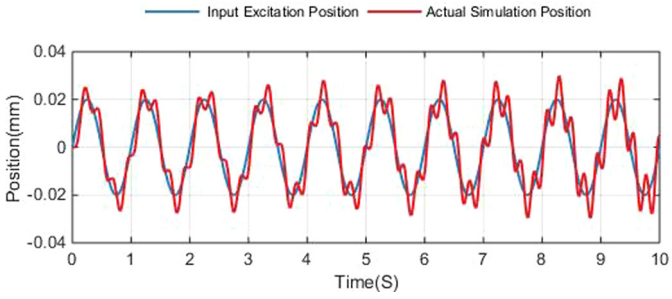

Fig. 10. Comparison between the input excitation and actual simulation position of the electric cylinder.

and the last two sections fit the stiffness curve. The fitting function defined:

$$\theta = \begin{cases} k1 \cdot T, & T \le T_1 \\ k_2 \cdot T + (k_1 - k_2) \cdot T_1, & T_1 \le T \le T_2 \\ k_3 \cdot T + (k_1 - k_2) \cdot T_1 + (k_2 - k_3) \cdot T_1, & T \ge T_2 \end{cases}. \tag{7}$$

When the torque is negative, the fitting function is symmetric with respect to the origin. Where, θ and T are the torsion angle and torque, respectively, k_1, k_2, $k_3$are the slopes of the fitted line, respectively, and $T_1$is the first inflection point of the piecewise curve. To reduce fitting parameters and improve the accuracy, the second inflection point T_2 is expressed as a function of T_1 and the slope. To minimise the error between superposition curve and median curve, nonlinear least square method based on Levenberg-Marquardt method is used to calculate the slope and inflection point of the three lines, respectively. The fitting line is shown in Fig. 9, and the fitting parameters are shown in Table 1.

The rated torque of ±3% is applied to the electric cylinder to overcome internal friction and oil film resistance. The input shaft angle is defined as the empty return clearance. As shown in Fig. 9, the two yellow dots are the data points corresponding to ±3% of the rated load. The angle difference between the two points is the total empty return clearance of the electric cylinder, with a value of 20.15 arcmin. At the same time, the two points are just at the first inflection point of the superposition line. It means that after two points, the components of the electric cylinder begin to contact, which proves the correctness of fitting and empty return clearance calculation.

Since the input end is only affected by the driving force and does not contact the load end during the empty return clearance, the data of the first linear segment cannot be used for stiffness fitting. When the internal contact of the electric cylinder is optimal, the fitting stiffness function is as follows:

$$\mathrm{C} = \begin{cases} \dfrac{1}{\mathrm{k_2}}, 0 \le T \le \mathrm{T_2} \\ \dfrac{1}{\mathrm{k_3}}, T \ge \mathrm{T_2} \end{cases}, \tag{8}$$

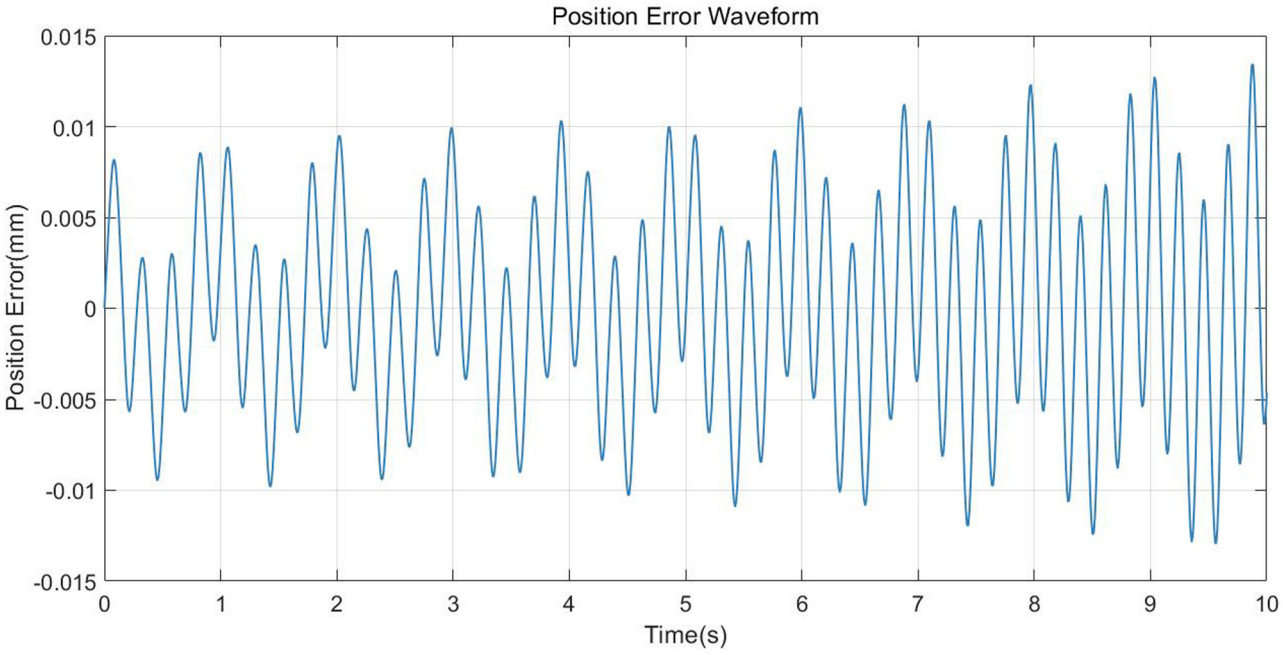

Fig. 11. Electric cylinder position error waveform.

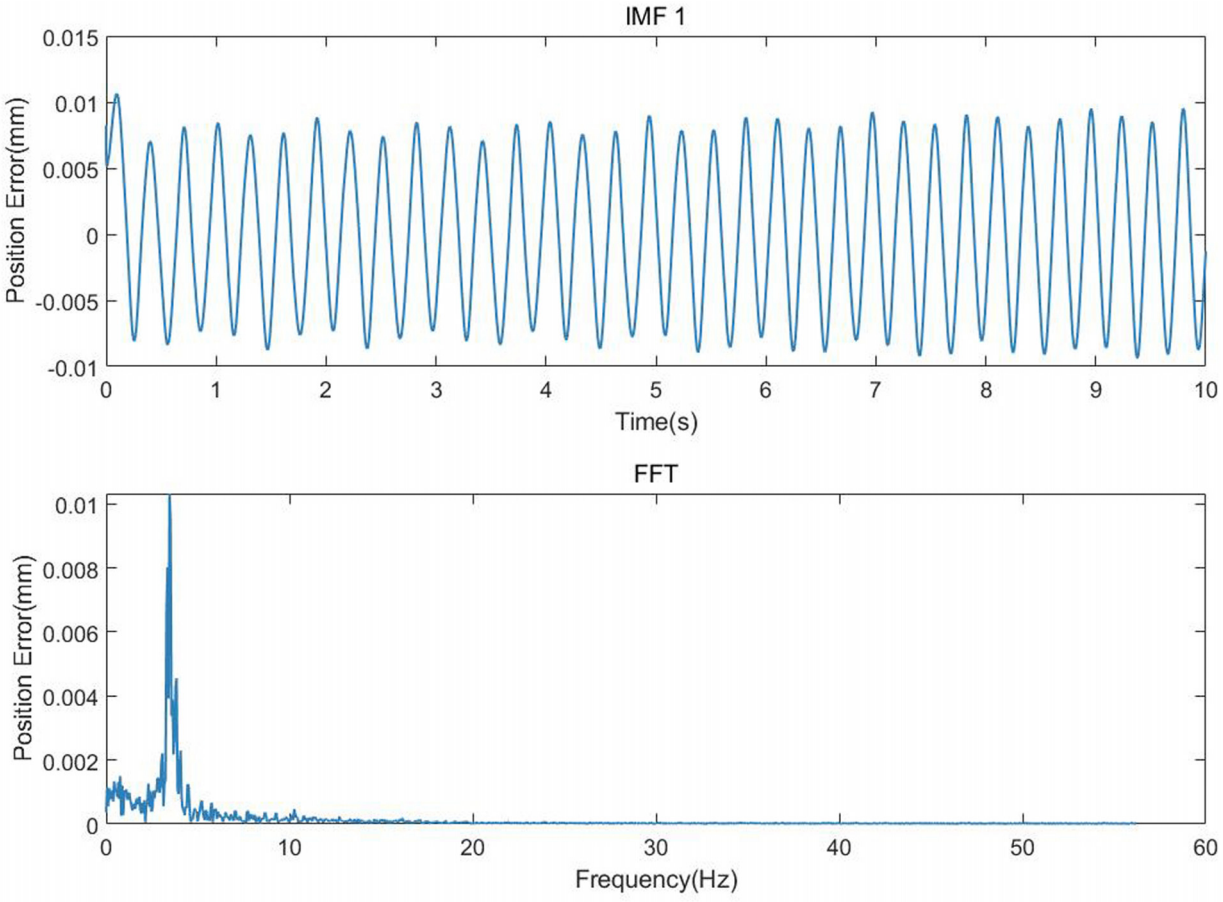

Fig. 12. First-order IMF and FFT analysis of position error.

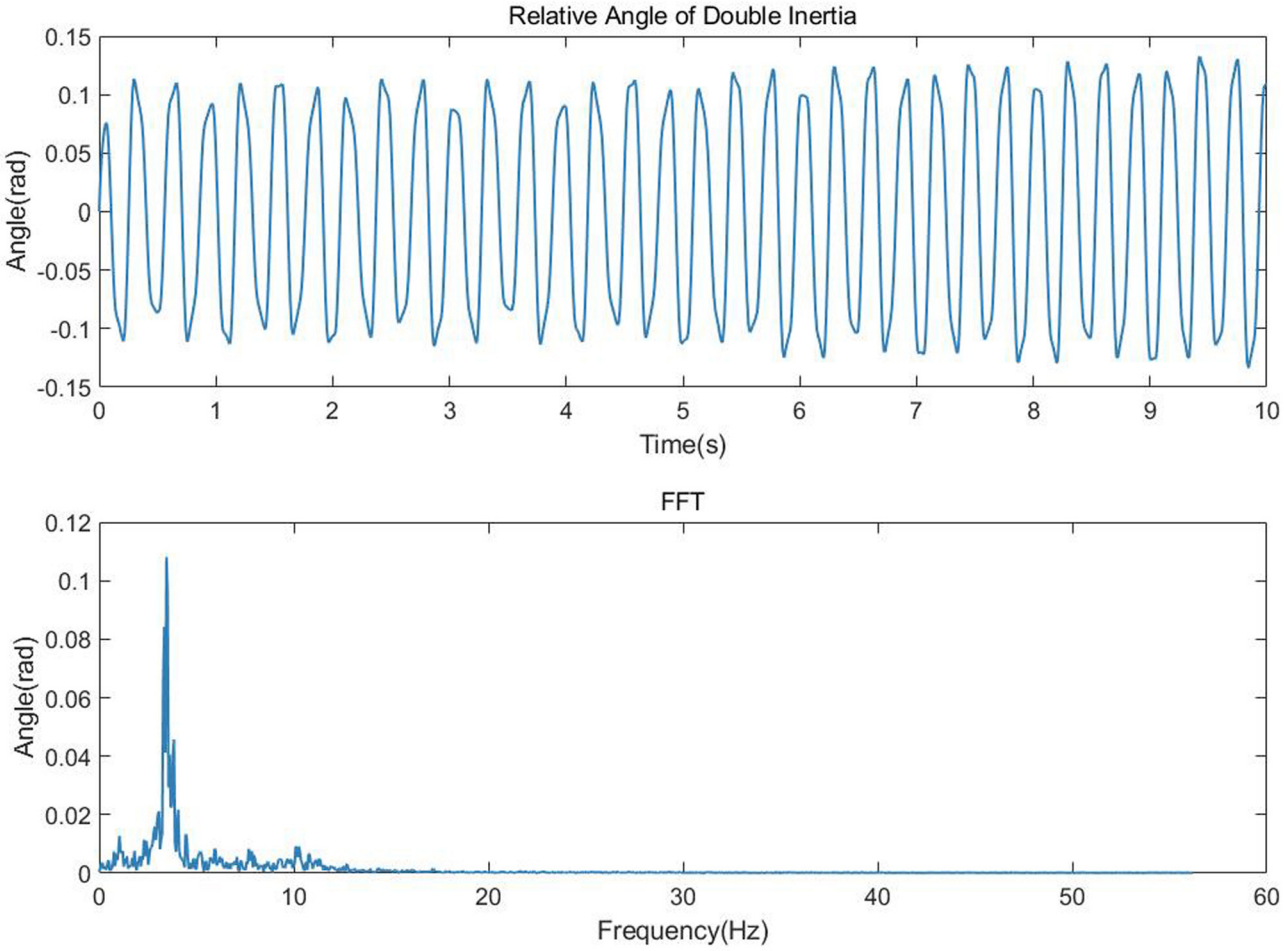

Fig. 13. Analysis of relative angle curve and its FFT.

It can be concluded that the transmission stiffness is not constant, but increases significantly as the load increases. When modelling the electric cylinder, not only should the nonlinear characteristics of the system be taken into account, but also the changes in load should be incorporated into the model.

4 Simulation and verification

4.1 Simulation and verification of the electric cylinder model

According to the model in section 2 and the key parameters of the model in section 3, the servo system based on the electric cylinder model is simulated and verified. The selection of controller model parameters, motor parameters and actual test parameters of the electric cylinder drive mechanism are shown in Table 2.

The parameters in Table 2 are substituted into the mathematical model in Fig. 6. The input excitation of the mathematical model is given as the desired position of the sinusoidal signal with amplitude of 0.02 mm and a frequency of 1Hz. The axial displacement of the model output is recorded. The results are shown in Fig. 10. It can be seen that when zero return clearance and stiffness nonlinearity are introduced, the actual simulation position will deviate from the expected input excitation position.

The error between the simulation position and the input excitation position is calculated as shown in Fig. 11. It can be seen that the position error is the superposition of multiple waveforms with different amplitudes and frequencies. The position error is decomposed into five Intrinsic Mode functions (IMF) by Empirical Mode Decomposition (EMD). Since the amplitudes of IMF_3 to IMF_5 are much smaller than the first two orders, they are ignored, and only the first two levels of IMF are considered. The decomposed IMF signal is transformed by fast Fourier transform to find its frequency domain component. The results are shown in Fig. 12.

Based on the monitoring of the process variables in the simulation, it can be found that the first-order IMF of the position error in Fig. 12 is similar to the relative angle $\Delta\theta$ waveform diagram between the double inertia in Fig. 13. Their main frequency components are about 3.45Hz. Therefore, the fluctuation of relative angle $\Delta\theta$ will cause dynamic error of the electric cylinder servo system.

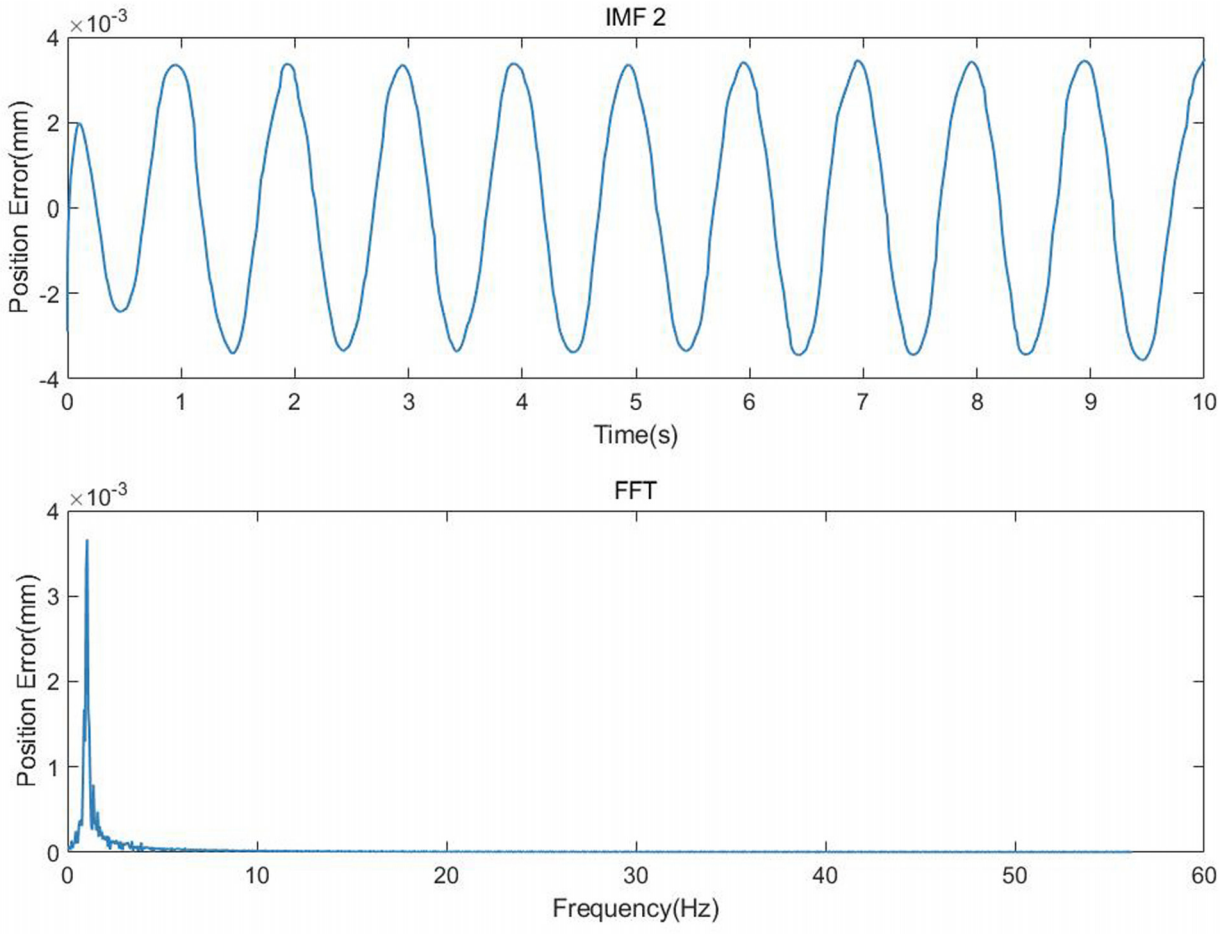

Fig. 14. Analysis of second-order IMF and its FFT.

As shown in Fig. 14, the frequency of IMF2 is about 1Hz, which is consistent with the expected position sine curve. The stable position error amplitude is converted into the angle error amplitude of the motor rotor by the ideal lead screw and gear pair. It is close to the unilateral empty return clearance of the electric cylinder. Therefore, when the motor rotates and reverses, due to the dead zone in the air return clearance, the driving components will briefly lose control, and the positioning accuracy of the electric cylinder will be affected by approximately constant static errors.

4.2 Sensitivity analysis of empty return clearance and stiffness on servo system accuracy

4.2.1 Sensitivity analysis of stiffness

Based on the effect of the relative angle $\Delta\theta$ on the dynamic error of the servo system, it is inferred that increasing the stiffness can reduce the amplitude of $\Delta\theta$. As shown in Fig. 15, when keeping other parameters constant and only changing stiffness, IMF1 waveform of the position error is used to analyse the influence of stiffness on error and sensitivity. Based on the output torque of the motor in the simulation, it is found that the torque in the system is located in the first stiffness zone under most working conditions. The piecewise stiffness function is reduced to a constant:

$$C = \frac{1}{k_2} \tag{9}$$

The stiffness of the first section is used as a unified evaluation standard. A simulated waveform of 1s is captured for observation. From Fig. 15, it can be seen that as the system stiffness increases, the position error amplitude of the servo system corresponding to IMF1 significantly decreases, and the system lag is significantly improved. The simulation results show that when the stiffness increases by 30%, the average position error can be reduced by 15%. The specific values are shown in Table 3.

4.2.2 Sensitivity analysis of transmission clearance

The same method is used to analyse the influence of empty return clearance, as shown in Fig. 16. Compared with stiffness, the sensitivity of error to empty clearance is much lower. Only when the empty return clearance increases or decreases by about 50%, the amplitude of IMF_2 will relatively change significantly. There are two reasons: on one hand, the empty return clearance is small. According to

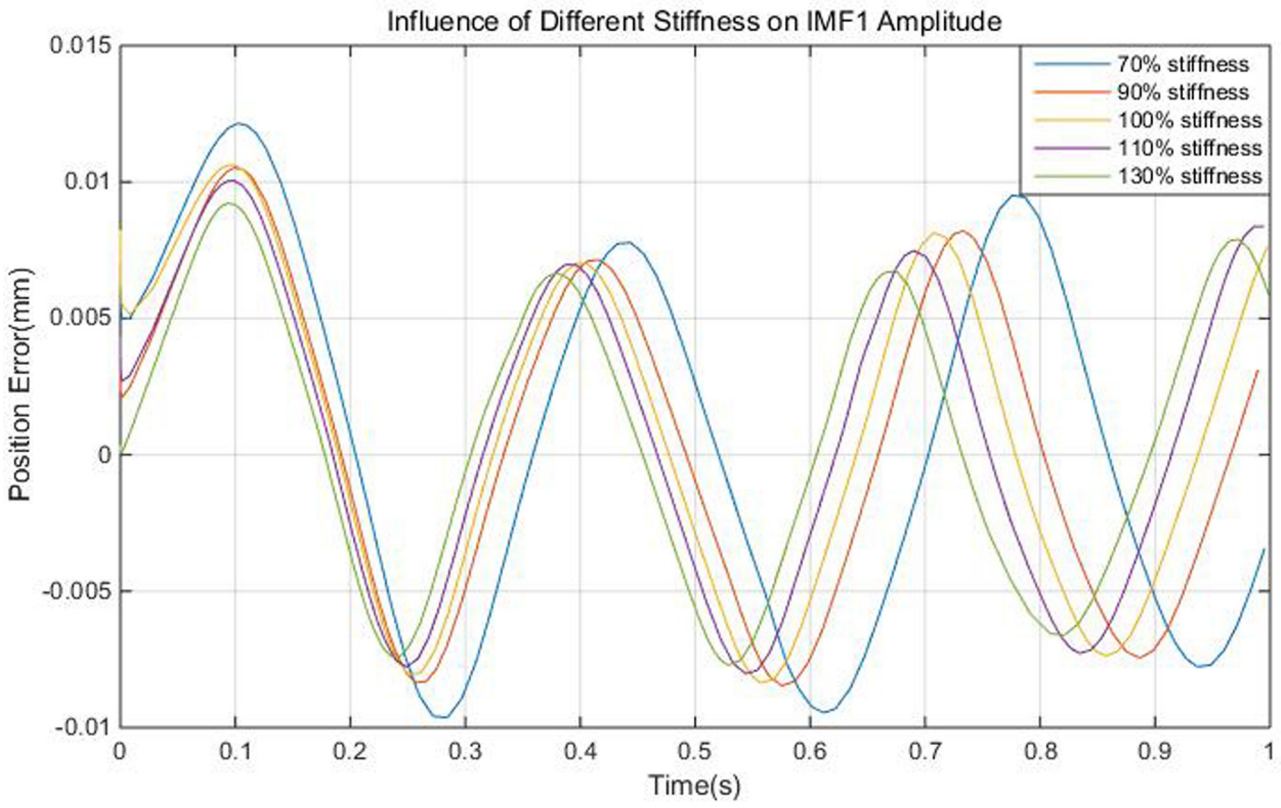

Fig. 15. Influence of different stiffness on IMF1 amplitude.

Table 3. Effect of system stiffness on servo system accuracy

Stiffness	Standard deviations of position error (mm)	Lag time after steady state(s)
70%	0.0065	0.125
90%	0.0058	0.083
100%	0.0054	0.055
110%	0.0052	0.026
130%	0.0049	0.010

the above EMD results, the amplitude of IMF_2 takes up a much smaller proportion in the error waveform than that of IMF_1; on the other hand, the empty return clearance has an important nonlinear characteristic in addition to the static error. A speed difference will occur when the driver and the follower experience an clearance dead zone. When the two are joined or in contact again, a large significant impact may occur, increasing the risk of dynamic errors and system shocks. This feature is not reflected in the model, which will also reduce the effect of the size of the empty return clearance on the systematic error.

5 Conclusion

In this paper, the influence of the electric cylinder driving characteristics on servo system accuracy is studied and analysed. Firstly, the servo motor model and transmission model of the electric cylinder are constructed, and the key parameter test device is set up. The experimental data are calculated and processed. The accurate measurement values of void clearance and stiffness are obtained directly from the actual system of the electric cylinder, and the model is modified. This process is more practical and novel than the previous research. By using these accurate data, the simulation model of the servo system of the electric cylinder that is more close to the reality is established in this paper. By using these accurate data, the simulation model of the servo system of the electric cylinder that is more close to the reality is established in this paper. On this basis, the root of the system error is deeply analysed, and the sensitivity of the empty return clearance and stiffness of the electric cylinder to the system error is discussed. The following conclusions are drawn. The conclusions are drawn as follows:

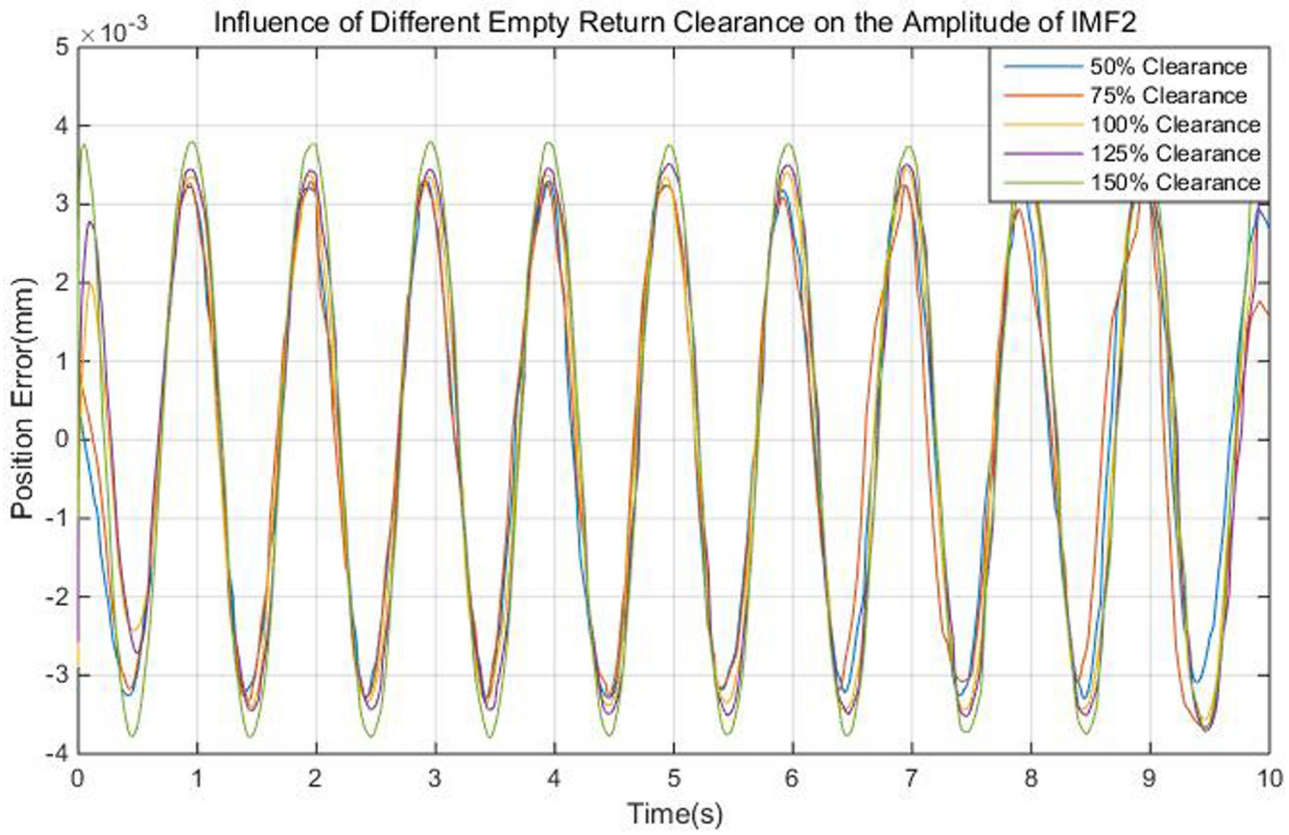

Fig. 16. Influence of different empty return clearance on the amplitude of IMF2.

– The system errors mainly come from the dynamic error caused by the deformation of internal components of the electric cylinder. The errors can be effectively reduced by increasing the system stiffness;
– Another source of system errors is the dead zone effect caused by the empty return clearance of the electric cylinder. This effect will cause the system consistently generatestatic errors with amplitude similar to the unilateral space return clearance. Without considering the nonlinear impact caused by the empty return clearance, reducing the clearance to improve system accuracy can be ignored.

The results can provide a support for modelling and optimal design of the electric cylinder servo system, as well as improving the accuracy of the electric cylinder servo system.

Funding

No funding was received for this work.

Conflicts of interest

We declare that we do not have any commercial or associative interest that represents a conflict of interest in connection with the work submitted.

Author contribution statement

Yang Lei: Design of methodology.
Yuanqing Xia: Formulation of overarching research goals.
Yiyang Huo: Performing the experiments and dada analysis.
All authors have read and approved the final version of the manuscript.

Data availability statement

The datasets used or analysed during the current study are available from the corresponding author on reasonable request.

References

[1] J. Yao, X. Cao, Y. Zhang, Y. Li, Cross-coupled fuzzy PID control combined with full decoupling compensation method for double cylinder servo control system, *J. Mech. Sci. Technol.* 32 (5), 2261–2271 (2018). https://doi.org/10.1007/s12206-018-0437-9
[2] D. Liu, J. Wang, S. Wang, D. Shi, Active disturbance rejection control for electric cylinders with PD-type event-triggering condition, *Control Eng. Pract.* 100, 104448 (2020). https://doi.org/10.1016/j.conengprac.2020.104448
[3] Y. Liu, X. Gao, X. Yang, Research of control strategy in the large electric cylinder position servo system, *Math. Probl. Eng.* 2015 (1), 167628 (2015). https://doi.org/10.1155/2015/167628

[4] A.K. Kumawat, R. Kumawat, M. Rawat, R. Rout, Real-time position control of electrohydraulic system using PID controller, *Mater. Today: Proc.* 47(Part 11), 2966–2969 (2021). https://doi.org/10.1016/j.matpr.2021.05.203

[5] Y. Yi, H. Qu, Y. Jian, H. Wang, N. Qu, Design of batch automatic testing system based on electric cylinder, *J. Phys.: Conf. Ser.* 2674 (1), 012006 (2023). https://doi.org/10.1088/1742-6596/2674/1/012006

[6] Y. Li, G. Chen, L. Chen, Rigid-flexible coupling dynamic modeling and characteristic analysis of the chain ramming mechanism, *J. Mech. Sci. Technol.* 36 (11), 5383–5397 (2022). https://doi.org/10.1007/s12206-022-1005-x

[7] H.L. Bartlett, S.T. King, M. Goldfarb, B.E. Lawson, Design and assist-as-needed control of a lightly powered prosthetic knee, *IEEE Trans. Med. Robot. Bionics* 4 (2), 490–501 (2022). https://doi.org/10.1109/TMRB.2022.3161068

[8] T. Wang, T. Zheng, S. Zhao, D. Sui, J. Zhao, Y. Zhu, Design and control of a series–parallel elastic actuator for a weight-bearing exoskeleton robot, *Sensors* 22 (3), 1055 (2022). https://doi.org/10.3390/s22031055

[9] R. Bhattacharjee, S. Kundu, S. Chaudhuri, Evaluation of workspace and coupled motions of an electrohydraulic parallel manipulator, in: *Proc. 2021 4th Int. Conf. Electr. Comput. Commun. Technol. (ICECCT)*, IEEE, Erode, India, 1–8 (2021). https://doi.org/10.1109/ICECCT52121.2021.9616672

[10] Y.H. Park, H.K. Lee, K.T. Park, H.C. Park, Practical behavior of advanced non-linear hydraulic servo system model for a mold oscillating mechanism depending on line volume, *J. Mech. Sci. Technol.* 30 (3), 975–982 (2016). https://doi.org/10.1007/s12206-016-0201-y

[11] D. Lin, G. Yang, Adaptive robust control for electric cylinder with friction compensation by LuGre model, Vibroengineering PROCEDIA, 39, 52–57 (2021). https://doi.org/10.21595/vp.2021.22182Z.

[12] Geng, Study on the position control of electric cylinder based on fuzzy adaptive PID, International Journal of Robotics and Automation, 35 (3), 242–247 (2020). 10.2316/j.2020.206-5226

[13] P.H. Gøytil, D. Padovani, M.R. Hansen, Linear time-invariant modelling of electrohydraulic cylinders, in: *Proc. 2022 Int. Conf. Electr. Comput. Commun. Mechatron. Eng. (ICECCME)*, IEEE, Maldives, 1–6 (2022). https://doi.org/10.1109/ICECCME55909.2022.9988490

[14] C.W. Mathews, D.J. Braun, Design of parallel variable stiffness actuators, *IEEE Trans. Robot.* 39 (1), 768–782 (2023). https://doi.org/10.1109/TRO.2022.3197088

[15] N. Verbanac, G. Jungmayr, E. Marth, N. Bulić, Reduced-order observer-based position control of a magnetic-geared servo drive, *Actuators* 13 (1), 6 (2024). https://doi.org/10.3390/act13010006

[16] Q. Zhang, R. Yu, C. Li, Y.H. Chen, J. Gu, Servo robust control of uncertain mechanical systems: application in a compressor/PMSM system, *Actuators* 11 (2), 42 (2022). https://doi.org/10.3390/act11020042

[17] F. Li, Y. Luo, X. Luo, P. Chen, Y. Chen, Optimal FOPI error voltage control dead-time compensation for PMSM servo system, *Fractal Fract.* 7 (3), 274 (2023). https://doi.org/10.3390/fractalfract7030274

[18] H. Yan, J. Li, L. Li, J. Ma, Research of active disturbance rejection controller design for PMSM servo system, *J. Phys.: Conf. Ser.* 1894 (1), 012039 (2021). https://doi.org/10.1088/1742-6596/1894/1/012039

[19] Y. Liu, Y. Wang, Y. Wang, An observer-based IT2 TSK FLS compensation controller for PMSM servo systems: design and evaluation, *Neural Comput. Appl.* 34 (13), 10949–10969 (2022). https://doi.org/10.1007/s00521-022-07020-y

[20] K.U. Yang, J.H. Byun, The synchronous control system design for four electric cylinders, *J. Korea Inst. Electron. Commun. Sci.* 11 (12), 1209–1218 (2016). https://doi.org/10.13067/jkiecs.2016.11.12.1209

Cite this article as: Y. Lei, Y. Xia, Y. Huo, Influence of Electric Cylinder Transmission Characteristics on Servo System, Mechanics & Industry **26**, 15 (2025), https://doi.org/10.1051/meca/2025010